BULLETIN OF THE EARTHQUAKE
RESEARCH INSTITUTE
Vol. 43 (1965), pp. 641-660

42. *Theoretical Seismograms of Spheroidal Type on the Surface of a Heterogeneous Spherical Earth.*

By Tatsuo USAMI, Yasuo SATÔ,
Earthquake Research Institute
and
Mark LANDISMAN,
Geosciences Division, Southwest Center for Advanced Studies.
(Read Sept. 28, 1965.—Received Sept. 30, 1965.)

1. Introduction

In a preliminary report of this study of theoretical seismograms for an earth model based on the velocities of Gutenberg and Bullen's A′ density distribution, results were presented for the fundamental radial mode of spheroidal oscillations[1]. It was there noted that these new results bear greater similarity to actual recordings of teleseisms than do previous calculations for more simplified spherical models, such as the homogeneous sphere[2] and the homogeneous mantle with liquid core[3].

The present study, which is part of a continuing program of investigation of the generation, propagation, dispersion and attenuation of waves in realistic spherical earth models, presents further results for the Gutenberg-Bullen A′ model. Theoretical seismograms representing the superposition of spheroidal oscillations were calculated, taking into account the contributions from free vibrations through the tenth radial mode, for all orders from the gravest with periods approaching one hour to those with periods slightly larger than one minute. The Common Spectrum used for these calculations is discussed, and comparison is

(Contribution No. 25 Geosciences Division, Southwest Center for Advanced Studies.)
(Contribution No. 869 Lamont Geological Observatory, Columbia University.)

1) T. USAMI, Y. SATÔ and M. LANDISMAN, "Preliminary Study of the Propagation of Spheroidal Disturbances on the Surface of a Heterogeneous Spherical Earth," *Geophys. J.*, (1965) (in press).

2) T. USAMI and Y. SATÔ, "Propagation of Spheroidal Disturbances on a Homogeneous Elastic Sphere, "*Bull. Earthq. Res. Inst.*, **42** (1964), 273-287.

3) Y. SATÔ and T. USAMI, "Propagation of Spheroidal Disturbances on an Elastic Sphere with a Homogeneous Mantle and a Core," *Bull. Earthq. Res. Inst.*, **42** (1964), 407-425.

made with the body waves predicted by ray optics.

Notable results of the study of the propagation of spheroidal disturbances in a Gutenberg-Bullen A′ earth model are:

1. Certain special segments of each of the series of free vibrations, as a function of order or colatitudinal mode number n, correspond to transition regions from one radial mode to the next higher one. Free vibrations associated with these segments have large displacements near the mantle-core boundary and the associated propagating waves resemble Stoneley waves along a plane fluid-solid boundary.

2. The group velocity curves for the lower radial modes exhibit well defined maxima and minima which correspond, in the case of the fundamental mode, to reported observations of surface waves.

3. Summation of the contributions of spheroidal oscillations for radial modes one through ten of this model leads to theoretical seismograms which exhibit waves reflected from and transmitted through the earth's core.

4. These seismograms also show the diffraction of seismic disturbances into the shadow zone.

5. Higher mode surface waves have been found which are mainly related to the second and third radial modes. These waves correspond primarily to the group velocity minimum and adjacent maximum of the third radial mode ($i=3$) for periods between 300 and 500 sec.

2. Glossary

Case I): The problem of a homogeneous sphere[2]

Case II): The problem of a homogeneous mantle and a homogeneous liquid core[3]

a: radius of the earth

b: radius of the core

C, U: phase and group velocities

E_S, E_T: radial and colatitudinal stress on the earth's surface

$f(t)$: time function of the external force

$f^*(p)$: Fourier transform of the function $f(t)$

i: radial mode number

j: unit of the imaginary number

k: $(=p/V_{so})$

m: degree of an associated Legendre function (azimuthal mode number)

n: order of an associated Legendre function (colatitudinal mode number)

${}_i p_n$: circular frequency of free oscillation

P_{difr}: P wave diffracted into the shadow zone by the core

(r, θ, φ): polar coordinates

$\widehat{r\theta}$: colatitudinal stress

$P_n^m(\cos\theta)$: associated Legendre function by Ferrers' definition

${}_i S_n^u$, ${}_i S_n^v$: Common Spectrum of radial and colatitudinal components of disturbance

S_{mn}, T_{mn}: coefficient of spherical surface harmonics in the expansion of radial and colatitudinal components of external force

t: time

(u, v, w): displacement in the r-, θ- and φ-directions

$U_n(r)$, $V_n(r)$: function giving the radial distribution of u and v

U_l, V_l: values of U_n, V_n at the depth where the integration is terminated

${}_i u_n$, ${}_i v_n$: contribution of a normal mode oscillation for the radial mode number i and the order number n

V_P, V_S: P and S wave velocities

V_{S0}: S wave velocity on the surface of the earth

$({}_i u_n)$, $({}_i v_n)$: $\sum_{i=1}^{i}\sum_{n=0}^{n} {}_i u_n$, $\sum_{i=1}^{i}\sum_{n=0}^{n} {}_i v_n$

$[{}_i u_n]$, $[{}_i v_n]$: $\sum_{n=0}^{n} {}_i u_n$, $\sum_{n=0}^{n} {}_i v_n$

$\{{}_i u_n\}$, $\{{}_i v_n\}$: $({}_i u_n)-({}_1 u_n)$, $({}_i v_n)-({}_1 v_n)$

α: ratio of the colatitudinal to the radial component of displacement on the surface

η: non-dimensional frequency of free oscillation $(=ka=pa/V_{S0})$

λ, μ: Lamé's constants

ρ: density

3. Earth Model

A discussion of the Gutenberg-Bullen A′ model used in this study was presented in the preliminary report[1] as well as a graphical representation of the distributions of velocities and density as a function of radius (Figure 1)[1]. For the sake of completeness, and to permit comparisons in the future, the numerical values of compressional velocity, shear velocity and density used in this study are presented in Table 1.

Table 1. Radial distribution of P and S wave velocities after Gutenberg and density for Bullen's model A′ used for calculation of theoretical seismograms. In the core, slight modifications described in the preliminary report were made before interpolation. Values of these quantities for every step of iteration were obtained from this table using Runge's interpolation method for unequal intervals.

Distribution of P and S Wave Velocities
and Density Within
the Gutenberg-Bullen A′ Earth Model
Adopted in the Present Study

Depth	Density	V_P	V_S	Depth	Density	V_P	V_S
0.0	2.84	6.30	3.55	2900.0	5.66	13.65	7.20
32.0	2.84	6.30	3.55	2900.0	9.70	8.00	0.00
32.0	3.32	8.16	4.65	3370.0	10.36	8.72	0.00
60.0	3.34	8.15	4.60	3500.0	10.51	8.90	0.00
100.0	3.38	8.00	4.40	3870.0	10.94	9.35	0.00
150.0	3.42	7.85	4.35	4000.0	11.09	9.50	0.00
200.0	3.47	8.05	4.40	4400.0	11.48	9.90	0.00
300.0	3.55	8.50	4.60	4470.0	11.55	9.95	0.00
413.0	3.64	9.06	5.00	4580.0	11.65	10.00	0.00
413.0	3.64	9.06	5.00	4790.0	11.79	10.07	0.00
500.0	3.87	9.60	5.30	4890.0	11.85	10.09	0.00
600.0	4.10	10.08	5.60	5051.0	11.94	10.11	0.00
700.0	4.30	10.50	5.90	5072.0	11.94	10.11	0.00
800.0	4.46	10.90	6.15	5072.0	11.94	10.11	0.00
900.0	4.57	11.20	6.30	5086.0	11.95	10.20	0.00
1000.0	4.65	11.40	6.35	5111.0	11.965	10.48	0.00
1200.0	4.77	11.80	6.48	5135.0	11.975	10.76	0.00
1400.0	4.89	12.05	6.62	5150.0	11.99	11.15	0.00
1600.0	5.00	12.30	6.75	5170.0	11.99	11.20	0.00
1800.0	5.11	12.55	6.85	5370.0	12.07	11.20	0.00
2000.0	5.22	12.80	6.94	5570.0	12.14	11.20	0.00
2200.0	5.32	13.00	7.01	5770.0	12.20	11.20	0.00
2400.0	5.42	13.20	7.10	5970.0	12.24	11.20	0.00
2600.0	5.52	13.45	7.20	6170.0	12.29	11.20	0.00
2800.0	5.61	13.70	7.23	6370.0	12.30	11.20	0.00
2880.0	5.65	13.70	7.205				

4. Fundamental Expressions

The spheroidal disturbances of an elastic sphere having radial heterogeneity can be expressed in terms of the polar coordinates (r, θ, φ). When the effect of gravity is neglected, these expressions become:

$$(u, v, w)=\frac{1}{2\pi}\int_{-\infty}^{\infty}(u(p), v(p), w(p))\exp(jpt)dp\,,$$

$$u(p)=\sum_{m,n}A_{mn}\cdot U_n(r)\cdot P_n^m(\cos\theta)\begin{matrix}\cos\\ \sin\end{matrix} m\varphi\cdot f^*(p)\,,$$

$$v(p)=\sum A_{mn}\cdot V_n(r)\cdot\frac{d}{d\theta}P_n^m(\cos\theta)\begin{matrix}\cos\\ \sin\end{matrix} m\varphi\cdot f^*(p)\,,$$

$$w(p)=\sum mA_{mn}\cdot V_n(r)\frac{P_n^m(\cos\theta)}{\sin\theta}\begin{matrix}-\sin\\ \cos\end{matrix} m\varphi\cdot f^*(p)\,, \tag{4.1}$$

where U_n and V_n satisfy the simultaneous differential equations

$$\frac{d}{dr}(\lambda X_n+2\mu\dot{U}_n)+\frac{\mu}{r^2}[4r\dot{U}_n-4U_n+n(n+1)(-U_n-r\dot{V}_n+3V_n)]+\rho p^2U_n=0\,,$$

$$\frac{d}{dr}\left[\mu\left(\dot{V}_n-\frac{V_n}{r}+\frac{U_n}{r}\right)\right]+\frac{\mu}{r^2}[5U_n+3r\dot{V}_n-V_n-2n(n+1)V_n]$$
$$+\frac{\lambda}{r}X_n+\rho p^2V_n=0\,,$$

$$X_n=\dot{U}_n+\frac{2}{r}U_n-\frac{n(n+1)}{r}V_n\,. \tag{4.2}$$

The dot ($\cdot$) means differentiation with regard to r, namely d/dr. It is possible to write the disturbances in the time domain which result from Fourier transformation of the radial, colatitudinal and azimuthal components of displacement as

$$u=\frac{1}{2\pi}\sum_{m,n}P_n^m(\cos\theta)\cdot\begin{matrix}\cos\\ \sin\end{matrix} m\varphi\int_{-\infty}^{\infty}\left(\frac{S_{mn}}{E_S}+\frac{T_{mn}}{E_T}\right)\cdot U_n(r)\cdot f^*(p)\cdot\exp(jpt)dp\,,$$

$$v=\frac{1}{2\pi}\sum_{m,n}\frac{d}{d\theta}P_n^m(\cos\theta)\cdot\begin{matrix}\cos\\ \sin\end{matrix} m\varphi\int_{-\infty}^{\infty}\left(\frac{S_{mn}}{E_S}+\frac{T_{mn}}{E_T}\right)\cdot V_n(r)\cdot f^*(p)\cdot\exp(jpt)dp\,,$$

$$w=\frac{1}{2\pi}\sum_{m,n}\frac{mP_n^m(\cos\theta)}{\sin\theta}\cdot\begin{matrix}-\sin\\ \cos\end{matrix} m\varphi\int_{-\infty}^{\infty}\left(\frac{S_{mn}}{E_S}+\frac{T_{mn}}{E_T}\right)\cdot V_n(r)\cdot f^*(p)\cdot\exp(jpt)dp\,, \tag{4.3}$$

In these expressions, S_{mn} and T_{mn} are the coefficients of spherical surface harmonics which are developed in the latitudinal and longitudinal expansion of the radial and tangential forces acting on the surface of the elastic sphere. In the present case, a purely radial stress was applied to a small circle around the pole. In this case, $m=0$, $T_{mn}=0$ and S_{mn} was replaced by S_n. E_S and E_T, the radial and tangential stresses at the free surface $r=a$, are written

$$E_S=(\lambda+2\mu)_a\cdot\dot{U}_n(a)+\frac{(\lambda)_a}{a}(2U_n(a)-n(n+1)V_n(a))\,,$$

$$E_T=(\mu)_a\cdot\left(\dot{V}_n(a)-\frac{1}{a}(V_n(a)-U_n(a))\right). \tag{4.4}$$

$E_S=E_T=0$ gives the condition of the free spheroidal oscillations. Equations (4.3) were evaluated by contour integration which showed that the displacements can be represented by superposition of the contributions from the poles corresponding to the free oscillations,

$$\begin{aligned} u=&\frac{j}{2}\sum_{i,n,m}P_n^m(\cos\theta)\cdot\begin{matrix}\cos\\ \sin\end{matrix} m\varphi\\ &\times\left[\left(\frac{S_{mn}}{dE_S/dp}\mp\frac{T_{mn}}{dE_T/dp}\right)\cdot U_n(r)\cdot f^*(p)\cdot\exp(jpt)\right]_{p=ip_n},\\ v=&\frac{j}{2}\sum_{i,n,m}\frac{d}{d\theta}P_n^m(\cos\theta)\cdot\begin{matrix}\cos\\ \sin\end{matrix} m\varphi\\ &\times\left[\left(\frac{S_{mn}}{dE_S/dp}\mp\frac{T_{mn}}{dE_T/dp}\right)\cdot V_n(r)\cdot f^*(p)\cdot\exp(jpt)\right]_{p=ip_n}. \end{aligned} \tag{4.5}$$

w has a similar form of expression. In this formula, the ${}_ip_n$ are the frequencies of free spheroidal oscillation of the earth.

5. Method of Calculation of Non-dimensional Frequency

Numerical solution of the simultaneous equations (4.2), under the conditions of zero stress on the surface, was used to find the non-dimensional frequency of spheroidal oscillations of the earth. The equations were integrated from the surface towards the center, assuming the radial displacement on the surface to be 1. The general procedure used for numerical solution was previously developed for the problem of a heterogeneous half space[4]; the method used for spheroidal oscillations is summarized below.

First, trial values of non-dimensional frequency $\gamma(=ka=pa/V_{so})$ and of $\alpha(=V_n/U_n$ at $r=a)$ were chosen. The values of $\dot{U}_n$ and $\dot{V}_n$ at the surface resulted from application of the boundary conditions of a stress-free exterior surface, $E_S=E_T=0$. Using these starting values of U_n, V_n, $\dot{U}_n$ and $\dot{V}_n$ at the surface, equations (4.2) were numerically integrated down to the core boundary for the velocities and densities given in Table 1. Since the rigidity of the core is assumed to be zero, the

4) Y. SATÔ, "Numerical Integration of the Equation of Motion for Surface Waves in a Medium with Arbitrary Variation of Material Constants," *Bull. Seism. Soc. Amer.*, **49** (1959), 57-77.

tangential stress $\widehat{r\theta}$ should vanish at the bottom of the mantle, though the calculated value of $\widehat{r\theta}$ on this boundary is usually not zero. The above condition at the core boundary, together with the condition that the displacements must vanish at great depth, were used as test criteria in a two-dimensional search for the unknown quantities, which are the frequency η and the surface ratio of displacements α.

For this two-dimensional search, the trial value of η was at first fixed and α was incremented repeatedly until the sign of $\widehat{r\theta}$ reversed. Interpolation was used to find the value of $\alpha=\alpha_1$ which made $\widehat{r\theta}_{r=b}=0$. Adopting this value of $\alpha=\alpha_1$, U_n was calculated for the depth where displacement was presumed to vanish. The trial displacement result, U_l, was then stored.

For the second direction of this search plan, the frequency η was incremented and the value of α_1 that produced $\widehat{r\theta}_{r=b}=0$ and the corresponding value of U_l were calculated and stored. After the reversal of sign of U_l, a similar interpolation was applied to find the combination of η and α_1 which permitted both $\widehat{r\theta}_{r=b}$ and U_l to vanish.

As the order number n increased, the depth where the disturbance actually vanished became shallower. Therefore, for large values of n, it was not necessary to continue the process of iteration down to the core. The calculation was stopped at an appropriate depth in the mantle. In this case, the non-dimensional frequency was found by using the requirement that both U_n and V_n vanish at the depth where the iteration was terminated.

The values of dE_S/dp are also necessary for evaluating the contributions of each mode (see equation (4.5)). These values were computed in a manner similar to that used for the torsional problem[5].

6. Phase and Group Velocities

The results of the above calculations were presented in the preliminary report[1] in the form of curves of frequency η versus order number n for the various radial modes. These frequencies were also used to calculate phase and group velocity curves, by employing the asymptotic formula

$$C=V_{so}\eta/(n+1/2)\,, \tag{6.1}$$

5) Y. SATÔ, T. USAMI, M. LANDISMAN and M. EWING, "Basic Study on the Oscillation of a Sphere V: Propagation of Torsional Disturbances on a Radially Heterogeneous Sphere. Case of a Homogeneous Mantle with a Liquid Core," *Geophys. J.*, **8** (1963), 44-63.

$$U = V_{so} d\eta/dn \,. \tag{6.2}$$

Numerical values of phase and group velocities thus obtained are given in Table 2.

Table 2. Phase and group velocities of the Gutenberg-Bullen A′ earth model.

T sec. \ i	C (Phase velocity) km/sec.					U (Group velocity) km/sec.		
	1	2	3	4	5	1	2	3
100	4.13	5.94	7.20	8.10	9.07	3.8_5	4.6_5	5.6_0
130				8.87	8.99			
200	4.62	7.22	8.58	8.76	11.04	3.6_0	5.7_5	
300	5.35	8.10	8.32	10.90		3.8_0	6.5_5	8.2_5
340								6.6_5
360							8.6_5	
400	6.00	8.06	8.92			4.4_0	8.6_0	6.7_0
500	6.45	8.03	9.61			5.0_5	7.3_5	7.0_5
600	6.70	8.42	10.45			6.2_0	5.6_5	6.5_5
650							5.3_0	
700	6.68	9.27	12.00			7.3_5	5.8_0	5.4_0
800	6.55	9.83				8.0_0	7.3_0	
900	6.42	10.18				8.2_5		
1000	6.26	10.42						

It was noted in the cited report that certain portions of the frequency-order number curves form transition segments from one radial mode to the next higher one. For free vibrations along these segments, it was also shown that the particle motion at the core boundary is large compared to that at the free surface, and the group velocity curves exhibit well defined maximum values. These vibrations correspond to Stoneley waves along the core-mantle boundary.

7. Common Spectrum

The Common Spectrum of the radial component of displacement is defined by

$${}_iS_n^u = \left(\frac{S_{mn}}{dE_S/dp} + \frac{T_{mn}}{dE_T/dp} \right) \cdot U_n(r) \cdot f^*(p) \,. \tag{7.1}$$

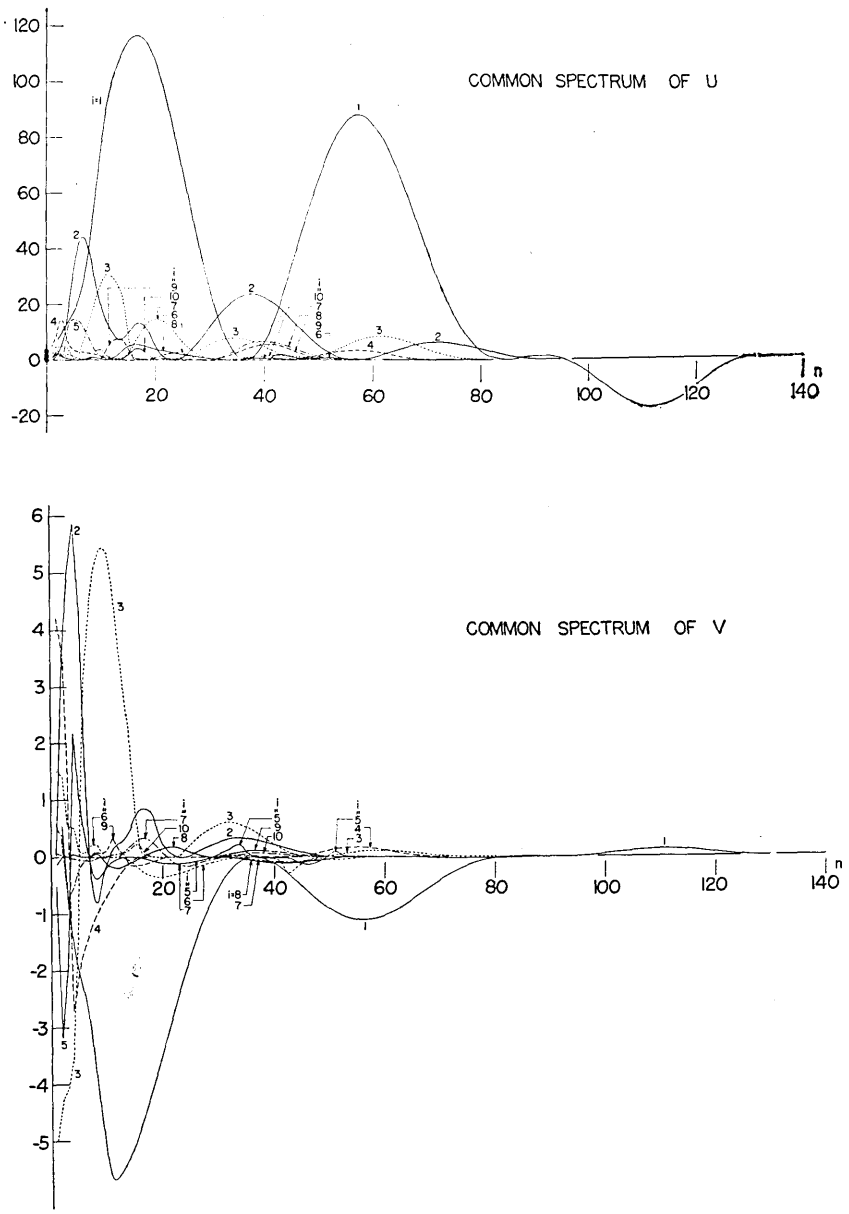

Fig. 1. Common Spectrum of radial and colatitudinal components of displacement. Values of radial component for $n=0$, $i=1, 2, \cdots, 10$ are indicated by solid circles.

The first expression of (4.5) is, therefore, reduced to

$$u=\frac{j}{2}\sum_{i,n,m}{}_iS_n^u\cdot P_n^m(\cos\theta)\begin{matrix}\cos\\ \sin\end{matrix} m\varphi\cdot\exp(jpt)\,. \tag{7.2}$$

This quantity ${}_iS_n^u$, is independent of quantities t, θ and φ, therefore it is common for the radial displacement expressions at all times and locations. Using the similar quantity ${}_iS_n^v$, the colatitudinal displacement v is expressed as

$$v=\frac{j}{2}\sum_{i,n,m}{}_iS_n^v\cdot\frac{d}{d\theta}P_n^m(\cos\theta)\begin{matrix}\cos\\ \sin\end{matrix} m\varphi\cdot\exp(jpt)\,. \tag{7.3}$$

Since axial symmetry was assumed in the actual computations, the azimuthal displacement w is zero. The Common Spectrum curves for the u and v components are shown in Figure 1. These curves become negligibly small for modes along the transition segments discussed in section 6. This result is consistent with the conclusion[1,3] that the transition segments exhibit behavior characteristic of boundary waves along the core-mantle interface. The marked differences between the results for this model and those for case II) (spheroidal disturbances on a homogeneous mantle) are:

1) for both components, the Common Spectrum of the higher modes does not decrease so rapidly with increasing n in the present case as in case II). In fact, quite complicated features in the Common Spectrum may be found, even for fairly large values of order number, n (see Figure 1).

2) In the present case, for the fundamental mode of both components the amplitude of the second peak is not much smaller than the first peak. In case of the homogeneous mantle the second peak is much smaller than the first.

8. Theoretical Seismograms

The source function was taken to be a purely radial stress applied at the surface. Its geographical distribution is

$$\Phi(\theta,\varphi)=\Phi^0(\cos\theta)=\begin{cases}1 & \theta<\theta_0\\ 0 & \theta_0<\theta\,.\end{cases}\qquad(\theta_0=0.04\text{ radian}) \tag{8.1}$$

The time function was taken to be

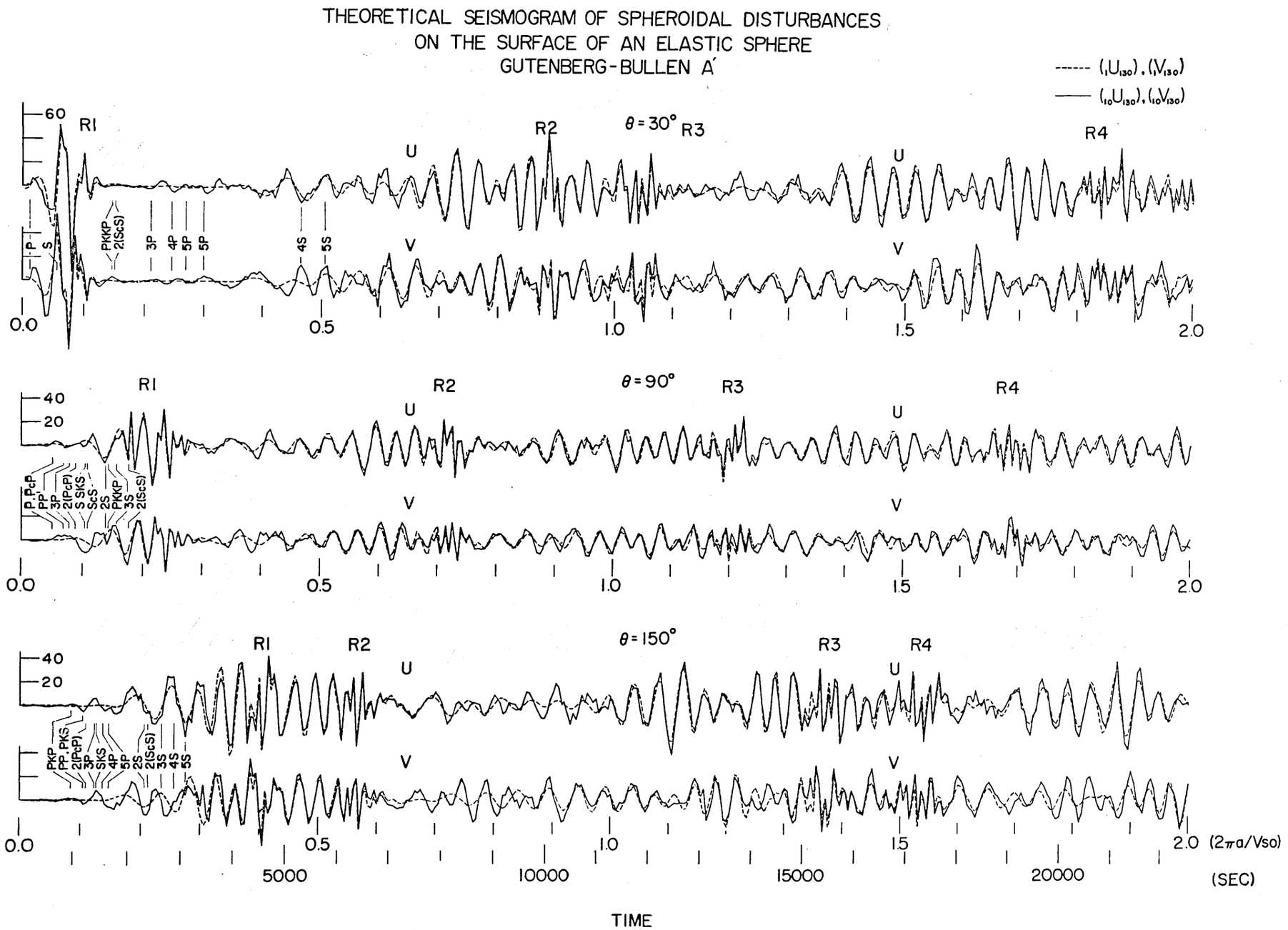

Fig. 2. Theoretical seismogram of spheroidal disturbances on the surface of a Gutenberg-Bullen A′ model of the earth due to a radial force around the pole. Arrows show the arrivals of various body wave phases. Solid line: ($_{10}u_{130}$) and ($_{10}v_{130}$). Broken line: ($_1u_{130}$) and ($_1v_{130}$). The unit of time was taken as (circumference of the earth)/(shear velocity on the surface).

$$f(t)=\begin{cases}-1 & -t_1<t<0\\ 1 & 0<t<t_1\\ 0 & t_1<|t|\,.\end{cases}\qquad (t_1=0.02) \tag{8.2}$$

and its Fourier transform is

$$f^*(p)=-4j\sin^2(pt_1/2)/p\,. \tag{8.3}$$

The largest values of colatitudinal order number n employed in the synthesis can be inferred from the curves in Figure 1. Beyond these values the spectral amplitude is small and contributions from these modes are negligible.

Theoretical seismograms were calculated at three points on the surface, namely

$$\theta=30^\circ,\ 90^\circ \text{ and } 150^\circ$$

for the time interval $t=0.005\ (0.005)\ 2.00$ and they are shown in Figure 2. The solid lines refer to $({}_{10}u_{130})$ and $({}_{10}v_{130})$ and the broken lines $({}_1u_{130})$ and $({}_1v_{130})$. $2\pi a/V_{S0}$, the time required for a shear wave to circle the globe, is taken as the unit of time.

These seismograms are more complicated and dispersive than those found for case II), and they realistically reproduce much of the character found in actual seismograms. Direct P and S waves, phases reflected from the core and the free surface, waves transmitted through the core and diffracted waves may be found in Figure 2. These waves can be more easily identified on the curves consisting of only higher modes (Figure 3). Figure 2 indicates that, as in case II), the fundamental mode is mainly related to the surface waves and the higher modes correspond to the body waves. However, this relation is not so close as in case II). In Figure 3, the summation of contributions from only the higher modes of the present elastic model displays a remarkable wave that has been named R_h. It is a representative example of a whole class of high velocity, dispersive, higher mode signals which arrive among and reveal the normal mode character of the ordinary teleseismic body waves. The amplitude of this wave is large near the poles and small near the equator, which is a property of surface waves. In order to make clear the nature of this wave, and to more clearly reveal the amount contributed by each radial mode to the various waves, Figure 4 was prepared. In this figure, the higher mode summations $\{{}_2u_{130}\}$, $\{{}_3u_{130}\}$, $\{{}_7u_{130}\}$, $\{{}_{10}u_{130}\}$, and corresponding colatitudinal component $\{{}_iv_n\}$ were plotted for epicentral distances $\theta=15^\circ$,

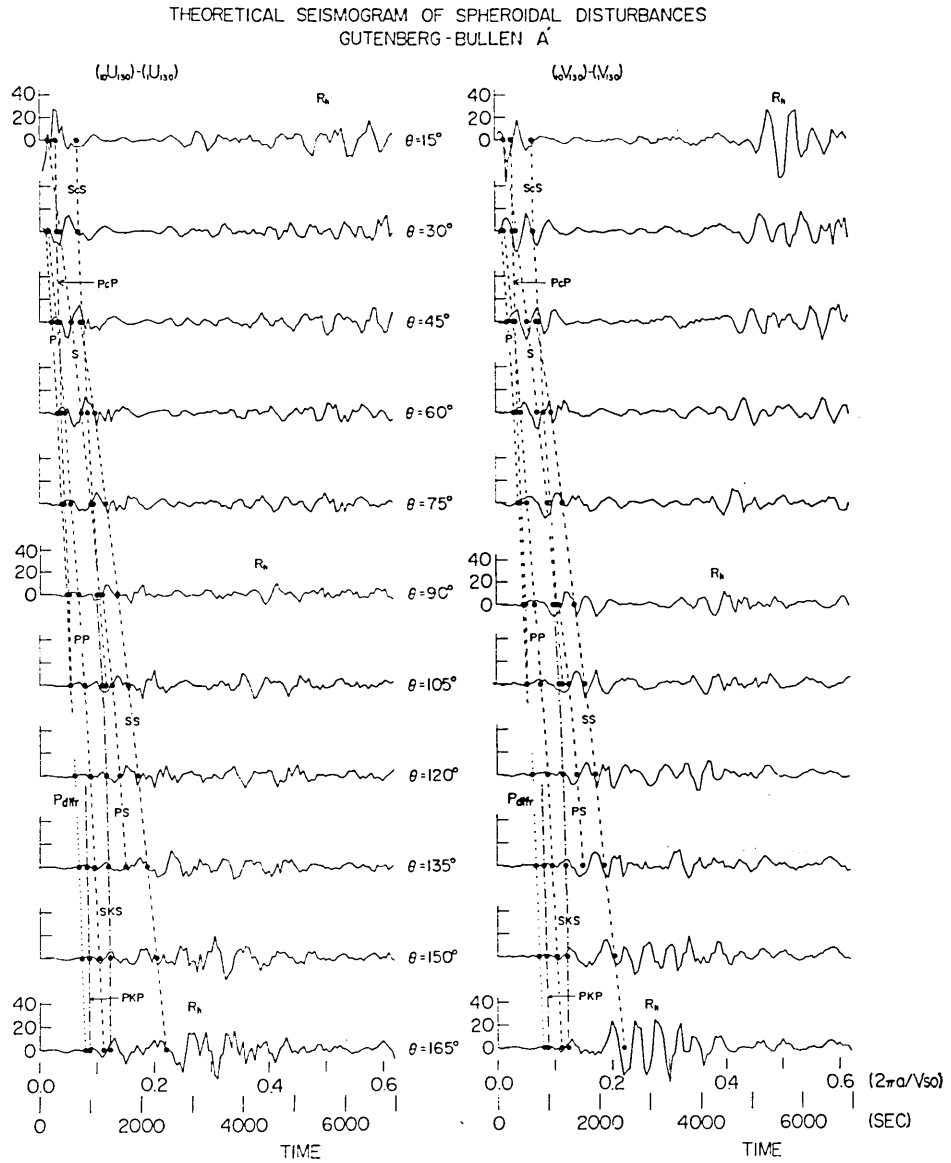

Fig 3. Radial and colatitudinal displacements computed for various epicentral distances. The curves show contributions of only higher radial modes. Solid circles are arrival times of body phases and broken lines indicate travel time curve of body waves. Note the diffraction of the *P* wave into the shadow zone caused by the core. Also note the predominant higher mode surface wave, which has large amplitudes near the pole and small ones near the equator.

45°, 90°, 135° and 165° where $\{{}_iu_n\}$ stands for $({}_iu_n)-({}_1u_n)$. Figure 4 shows that the colatitudinal component of R_h wave is mainly related to the radial mode $i=3$, while the radial component is the effect of mixture of contributions, primarily from radial modes $i=2$ and 3. The wave form of the colatitudinal component exhibits more regularity than does the radial component and the beginning of this wave can clearly be identified on the curves showing $\{{}_3v_{130}\}$, especially for $\theta=15°$ and 45°. The travel time of the onset of this wave coincides well with that to be expected

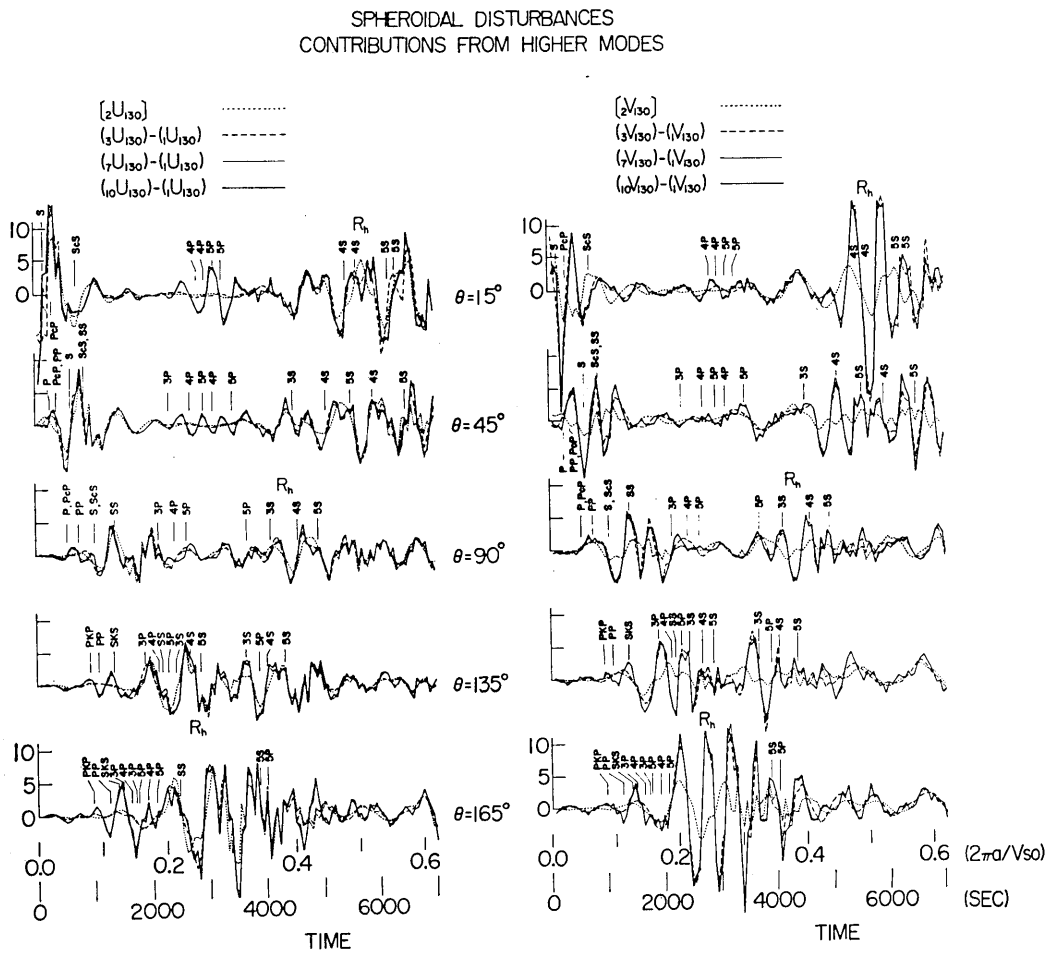

Fig. 4. Theoretical seismogram showing the contributions of higher modes. The degree of contributions of each radial mode to various kinds of waves is seen in this figure.

for a wave having the maximum group velocity associated with the radial mode $i=3$ for periods near 500 sec., which is approximately 7.0 km/sec. Judging from the characters of the R_h wave described above, it might be possible that this wave could be found on the horizontal component of ordinary teleseismic recording.

As is in the cases I) and II), the S waves can be expressed by the sum of contributions of comparatively low order radial modes, while contributions of high order radial modes must be added to express the P waves and core phases. These relations are well exhibited in Figure 4, especially in the seismogram of radial component.

As noted in the preliminary report[1], the Rayleigh waves end abruptly at the travel time corresponding to the minimum group velocity of the fundamental mode, $U_{\min}=3.57$ km/sec.

The disturbances diffracted by the core into the shadow zone may be identified on the theoretical seismograms (Figure 3). These waves arrive before the core phase *PKP*. The body phases cannot be so clearly identified on the seismograms as in case II), because the various body wave arrivals follow successively and overlap each other. The amplitude of the initial motion as a function of distance is shown in Figure 5.

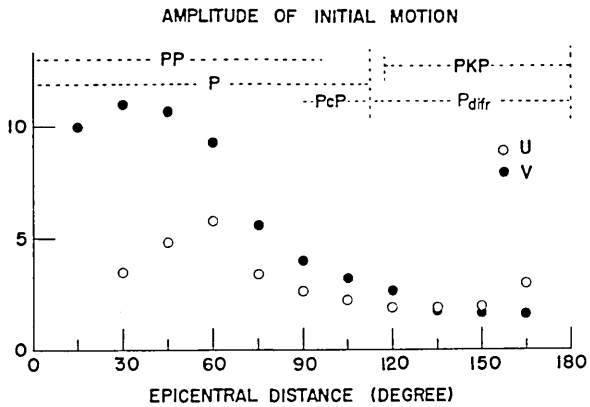

Fig. 5. Amplitude of initial wave as a function of epicentral distance. Open circle: radial displacement. Solid circle: colatitudinal displacement. Name of body phases mean the range in which these waves appear as or immediately after the initial wave.

9. Travel Time Curves

The travel times of various phases for an impulsive source at the

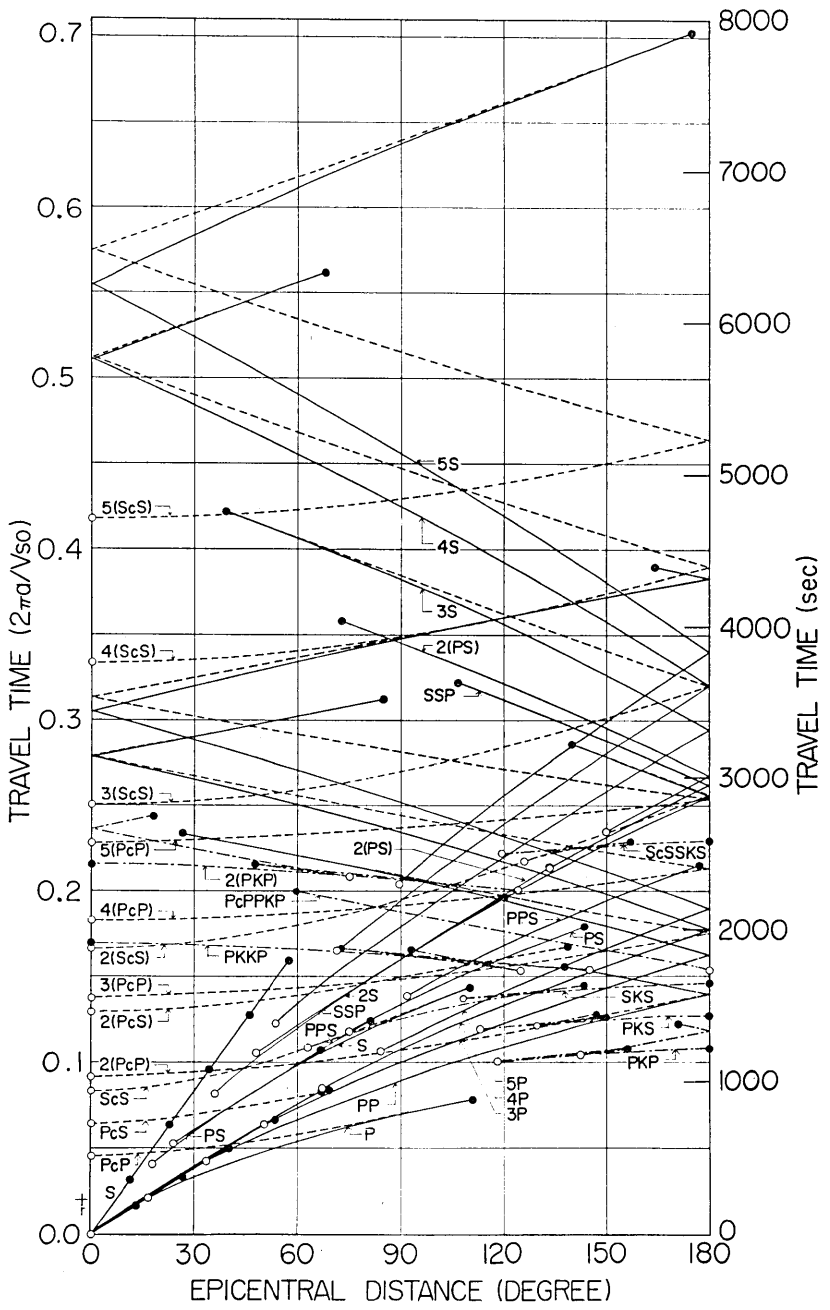

Fig. 6. Travel time curves of various body waves for an impulsive source at the pole, using Gutenberg's velocities. Cross on the lower left is the reference point in the present case. Solid line: direct P and S, and waves reflected at the surface only. Broken line: waves reflected at the core boundary. Chain line: waves passed through the core. Open and solid circles show the starting and end points of the various phases.

pole were computed for the velocities adopted in the present study and the results are given in Figure 6. The cross on the lower left is the reference point for the present case of a circular radial stress near the pole. Open and solid circles show, respectively, the starting and end points of the various phases. Travel time curves for the direct P and S waves and for waves reflected only at the surface have a shadow zone corresponding to Gutenberg's low-velocity layer in the mantle. Calculated travel times are shown in Figures 2 and 4 by arrows. The agreement between the expected arrivals and the actual appearance of the phases is satisfactory.

Appendix

Figures 7, 8 and 9 were reproduced here from the preliminary report[1] to make this study more understandable.

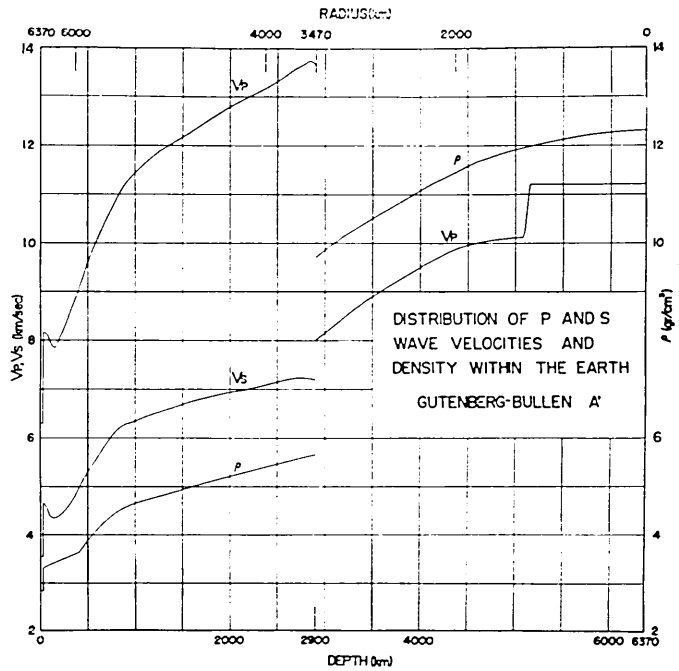

Fig. 7. Distribution of P and S wave velocities and density employed in this study.

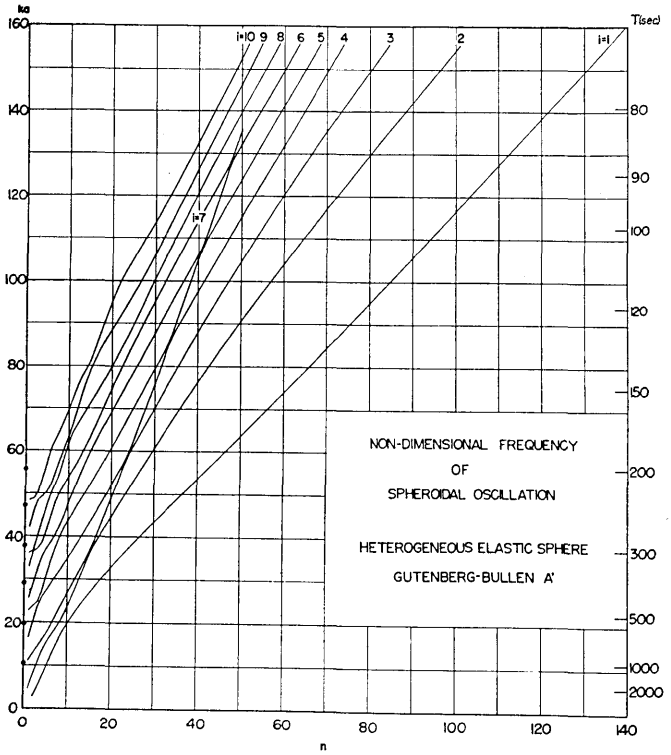

Fig. 8. Non-dimensional frequency of the free spheroidal oscillations of the Gutenberg-Bullen A′ earth model depicted in Fig. 7. For $n=0$, the results are shown as solid circles. Time unit as in Fig. 2.

Acknowledgements

The authors are greatly indebted to Professor Robert Jastrow, Director of the NASA Institute for Space Studies, for his generous hospitality and provision of computer facilities. Computing Facilities were also generously furnished by the Southern Methodist University Computing Laboratory. A part of the calculation was done through the project UNICON, IBM Japan.

The authors wish to thank the Geosciences Division of the Southwest Center for Advanced Studies and the Lamont Geological Observatory of Columbia University for permitting one of us, T. Usami, to visit these institutions while on leave from the Earthquake Research Institute of the University of Tokyo during the period of this study. We also are

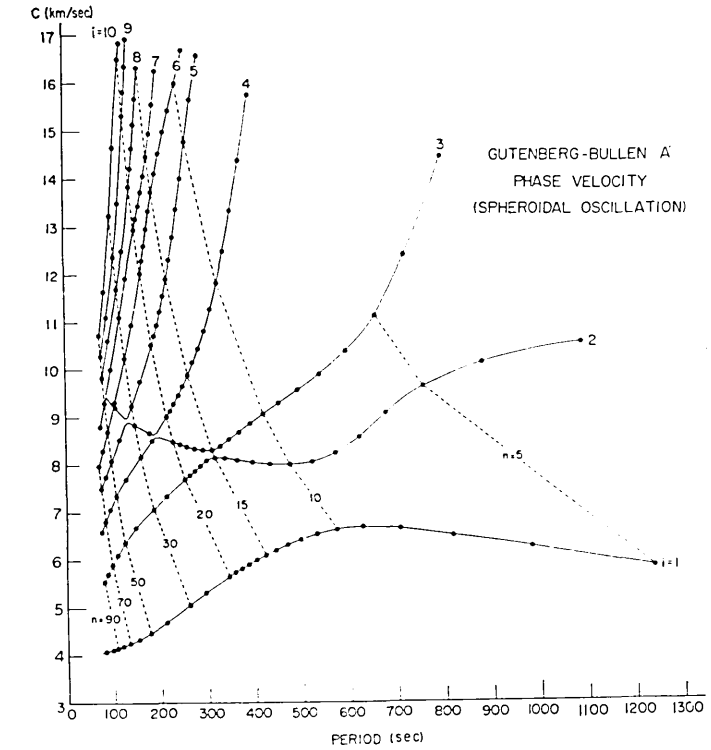

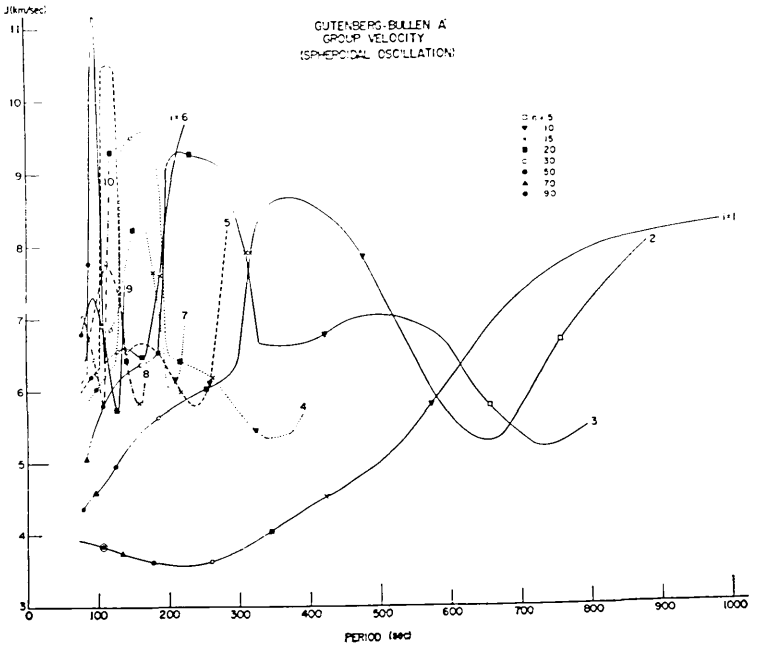

Fig. 9. Phase and group velocities as functions of period.

grateful to the Geosciences Division and the Earthquake Research Institute for helping to arrange a similar visit by Y. Satô.

This study was supported by the National Aeronautics and Space Administration, under contract NsG-269-62 with the Southwest Center for Advanced Studies, by supplemental research funds of the latter institution, and by the Air Force Office of Scientific Research contract AFOSR 62-303 with the Lamont Geological Observatory, as part of Project VELA Uniform sponsored by the Advanced Research Projects Agency.

---

42. 不均質弾性球の表面を伝わるスフェロイド型振動
——グーテンベルグ・ブレン A′ モデルの場合——

地震研究所 宇佐美 竜 夫
地震研究所 佐 藤 泰 夫
Southwest Center for Advanced Studies Mark LANDISMAN

1. 筆者らは弾性球を伝わる擾乱の理論地震記象の研究をつづけて来たが，今回はその一環として現実的な地球の表面を伝わるスフェロイド型擾乱について計算をした．方法は従来と同じで，変位を自由振動の各モードの和として表わした．

2. 地球モデルとしては，グーテンベルグの速度分布，ブレンの密度分布 A′ を採用した．地殻は V_P=6.30 km/sec, V_S=3.55 km/sec で厚さは 32 km，低速層を考え，密度の 2 次不連続の生じる深さは 413 km，核までの深さ 2900 km，核の内側での V_P=8.0 km/sec，内核と外核の境界層の半径は 1298，及 1200 km で，この間で V_P を急に変化させ，核を通る波の走時がグーテンベルグの求めたものと一致するようにした．地球の半径は 6370 km.

3. まず，スフェロイド型の自由振動の周波数を n=0(1)130, i=1(1)10 の各モードについて計算した．計算は各 i について周期の長い方から 75 秒までのモードについて行なつた．この周波数を各 i について n の函数として書くと，あるモードから次のモードへの遷移がはつきり認められる．この遷移分枝上のモードの振幅分布をみると，核の境界で振幅が急に大きくなり，その傾向は n が大きいほどはなはだしい．これは，このモードが固体と液体の境界面に沿うストンリー波に似た性質を持つていることを示す．ついで群速度と位相速度を求めた．i=1, 2 については位相速度に極大と極小が現われた．また基準振動の群速度は周期 220 sec で極小値 3.57 km/sec となる．この値はエアリー相の観測から得られた値と一致する．また上述の遷移分枝に相当し，位相速度には遷移が，群速度には幅の狭い極大が表われる．さらにスペクトルのうち観測点の位置と時刻に無関係な部分をコモン・スペクトルとして図示した．基準振動のスペクトルの第二の山は第一の山に比してわずか小さい．しかし，流体核を持つ等質等方マントルの場合には，第二の山は第一の山に比して非常に小さかつた．

4. 実際の計算に当つては重力の影響を無視し，軸対称 (m=0) を仮定した．外力としては極のまわりに次のような半径方向の力だけが働くと仮定した．

$$\Phi(\theta,\varphi)=\Phi^0(\cos\theta)=\begin{cases}1 & \theta<\theta_0\\ 0 & \theta>\theta_0\end{cases}\quad(\theta_0=0.04\ \text{ラヂアン})$$

$$f(t)=\begin{cases}-1 & -t_1<t<0,\\ 1 & 0<t<t_1\\ 0 & t_1<|t|\end{cases}\qquad(t_1=0.02)$$

時間の単位としては (周長)/(地殻の S 波速度)=11268 秒をとり，地球上の数点で時間 $t=0.0(0.005)2.0$ について計算した．

5. また，いろいろな実体波の走時を，この地球モデルについて計算をし，走時曲線を図示した．

6. 以上の計算の結果，次のことがわかつた．

a) 計算から求めた直達波の走時は，理論地震記象に見られる各波の発現時とよく一致する．

b) 核の陰での回折波が，高調波だけの和を示した理論地震記象に見られる．

c) 核での反射波，核内を通る波，その他の実体波は，明りようではない．これは，いろいろな実体波が次々に表われ，お互いに重り合う結果と考えられる．

d) 基準振動は表面波をよく表わしている．また，高次の振動は実体波と関係しているが，その関係は，流体核をもつ等方等質マントルの場合ほど密接ではない．

e) 高次の振動の和を示した理論地震記象に，表面波の性質（極の近くで振幅が大きく，赤道近くで小さい）を持つた著しい波（R_k 波と名づける）が見られる．この波は v 成分にはつきり現われ，$i=3$ の最大群速度に相当するもので $\{{}_3v_{130}\}$ の図をみると，そのはじまりが理論記象上によく示されている．

f) S 波は低次高調波で表わされるが，P 波は高次高調波まで加えなければ表わせないこと，等質等方マントルの時と同じである．

g) 群速度に極小値があるのに対応し，短周期波に着目すると，表面波の終りの点がはつきり，理論地震記象上にみいだされる．

7. 初動の振幅を震源距離の函数として示した．